Monte Carlo studies of nonequilibrium phonon effects in polar semiconductors and quantum wells. I. Laser photoexcitation

P. Lugli
Dipartimento di Ingegneria Meccanica, Seconda Università degli Studi di Roma, Tor Vergata, via Orazio Raimondo, I-00173 Roma, Italy

P. Bordone and L. Reggiani
Dipartimento di Fisica e Centro Interuniversitario di Struttura della Materia dell'Università degli Studi di Modena, via Campi 213/A, I-41100 Modena, Italy

M. Rieger and P. Kocevar
Institut für Theoretische Physik, Universität Graz, Universitätsplatz 5, A-8010 Graz, Austria

S. M. Goodnick
Center for Advanced Material Research, Oregon State University, Corvallis, Oregon 97331
(Received 11 October 1988)

The present paper illustrates a series of theoretical results on nonequilibrium phonon effects based on a novel Monte Carlo algorithm. The details of the numerical procedure are given. No assumptions on the form of the phonon or the electron distributions are required. The main emphasis is given to the study of LO-phonon perturbations as a result of the relaxation of photoexcited carriers in polar semiconductors. Bulk GaAs and InP, as well as GaAs-$Al_xGa_{1-x}As$ heterostructures are analyzed. Good agreement is found with available experimental results from time-resolved luminescence and Raman measurements. The strong phonon emission by the high-energy photoexcited electrons in the first stage of their relaxation (within a few tenths of a picosecond) is found to drive the phonon distribution strongly out of equilibrium. After the excitation, reabsorption of the emitted phonons by the carriers and nonelectronic phonon-decay processes bring the distribution back to its equilibrium value.

I. INTRODUCTION

The question of possible effects of nonequilibrium optical-phonon distributions on the dynamics of optically excited charge carriers in semiconductors is becoming a widely investigated and debated topic.[1-8] The main scientific motivation comes from the rapid development of picosecond and subpicosecond laser spectroscopy, which allows us to study even the fastest relaxation phenomena in solids and thereby also some fundamental hot-carrier–hot-phonon processes which might ultimately limit the switching efficiencies of ultrafast electronic devices. The energy-loss rates of nonequilibrium hot carriers in semiconductors determine their stability properties in high-field transport and also the effectiveness of the surface excitation and annealing by laser pulses. As the excited carrier system loses its energy mainly through emission of phonons, the mean phonon occupation number of the most strongly coupled vibrational modes will increase over its thermal equilibrium Planck distribution N_L at the lattice temperature T_L. This phonon amplification will ultimately depend on the rate at which the perturbed modes dissipate their excess energy by way of phonon-decay processes into the "heat bath" of the electronically inactive lattice modes. Figure 1 shows the energy flow to, within, and out of a coupled carrier-phonon system for the most general case of several types of carriers and electronically active phonons: electrons in different conduction-band valleys of Γ, L, and X symmetry, long-wavelength longitudinal-optical (LO) and transverse-optical (TO) phonons, and the remaining types of intervalley and acoustical phonons. Depending on the material, on the excitation level, and on temperature, different types of carriers, lattice modes, and carrier-phonon (c-ph) coupling will dominate the overall energy transfer from the external dc or laser field into the lattice. Direct experimental evidence for strongly amplified optical-phonon distributions has come from time-resolved Raman spectroscopy. The ensuing feedback of energy into the carrier system through the relative increase of phonon reabsorptions has been only indirectly evidenced through a heavily reduced cooling rate of highly laser-pulse-excited electron-hole systems.[1-4] However, for the high carrier concentrations involved in most of these experiments, possible contributions of carrier-carrier (c-c) scattering, screening of long-range c-ph couplings, spatial carrier diffusion, and collective plasma effects have not allowed an unambiguous separation of hot-phonon effects from the experimental data. Great efforts are therefore presently undertaken towards a sufficiently accurate theoretical description of highly excited c-ph systems to achieve deeper insights into the

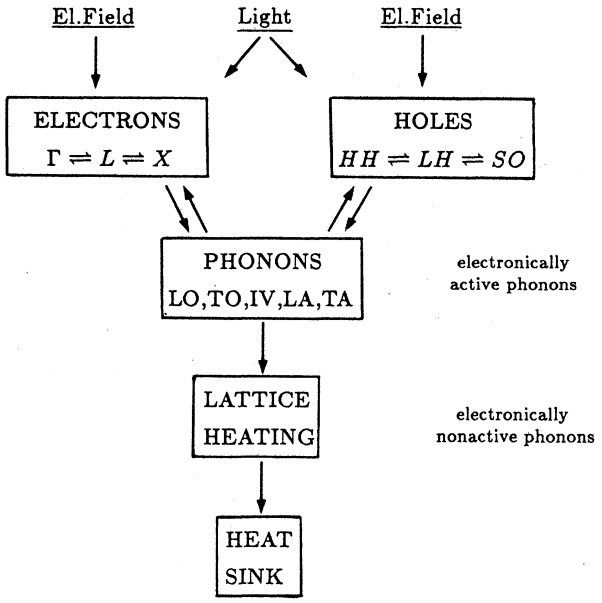

FIG. 1. Schematic representation of the energy flux in a typical semiconductor.

transient high-field response of semiconductors and solids in general. The best-suited framework for such investigations is the semiclassical transport theory, and most of the work on hot phonons has indeed been formulated in terms of the Boltzmann equation for the phonons, but always with simplifying assumptions about the functional form of the distribution function of the carriers.[9–13]

The purpose of the present work is to improve on these theories by doing away with the above restrictions through the use of Monte Carlo techniques, which should furthermore allow a more detailed study of the effectiveness and time scales of the individual microscopic scattering processes. The corresponding transport model for the carriers and optical phonons is set up in Sec. II. Our Monte Carlo algorithm for its solution is presented in Sec. III, with the appropriate specialization to the following applications to the photoexcitation of polar semiconductors: the simplified case of monoenergetic electron excitation in bulk GaAs and GaAs/$Ga_{1-x}Al_xAs$ quantum wells in Sec. IV, and the realistic case of electron excitation out of the threefold valence band of GaAs and InP in Sec. V, for which a direct comparison of our results with existing experimental data is possible.

II. THE TRANSPORT MODEL

The dynamical evolution of the carrier-phonon system under space-homogeneity conditions can be adequately described by the coupled Boltzmann equations:

$$\frac{\partial f_{\mathbf{k}}}{\partial t}=\frac{\partial f_{\mathbf{k}}^{(i)}}{\partial t}\bigg|_{c\text{-ph}}+\frac{\partial f_{\mathbf{k}}^{(i)}}{\partial t}\bigg|_{c\text{-}c}+\frac{\partial f_{\mathbf{k}}^{(i)}}{\partial t}\bigg|_{c\text{-impurity}}, \quad (1)$$

$$\frac{\partial N_{\mathbf{q}}^{(j)}}{\partial t}=\frac{\partial N_{\mathbf{q}}^{(j)}}{\partial t}\bigg|_{\text{ph-}c}+\frac{\partial N_{\mathbf{q}}^{(j)}}{\partial t}\bigg|_{\text{ph-ph}}, \quad (2)$$

where $f_{\mathbf{k}}$ and $N_{\mathbf{q}}$ are, respectively, the carrier and the phonon distribution functions. The superscripts i and j indicate, respectively, the type of carrier (electrons or holes) and of phonon modes (LO, TO, ...) considered. In the following, only electrons will be considered. Such an assumption is justified as long as the carrier densities are not too high, so that no efficient coupling exists between electrons and holes (electron concentrations always lower than 5×10^{17} cm^{-3} will be dealt with in the paper). In the same spirit, we assume unscreened electron-phonon interactions.

The time-dependent transport equations for carriers and phonons are coupled through the occurrence in the carrier-phonon collision integrals of both carrier and phonon distribution functions.[9] A decisive simplification of the phonon equation comes from the possibility of using a temperature-dependent relaxation time for the phonon-phonon interactions, τ_{op}, in the form

$$\frac{\partial N_{\mathbf{q}}}{\partial t}\bigg|_{\text{ph-ph}}=-\frac{N_{\mathbf{q}}-N_L}{\tau_{\text{op}}}, \quad (3)$$

where N_L is the thermal Planck distribution

$$N_L=(e^{\hbar\omega/k_BT_L}-1)^{-1} \quad (4)$$

and $\hbar\omega$ is the phonon energy.

The relaxation-time approximation is justified by the fact that the phonon-phonon interactions are dominated by the decay of the LO phonons into pairs of electronically nonactive phonons from zone-boundary modes. Zero-temperature values of the phonon lifetime, τ_{op}, are generally of the order of 10 ps, with a weak decrease with temperature.[14,15] Time-resolved phonon spectroscopy has yielded a rather wide range of values for τ_{op}, between 7 ps (Ref. 16) and 28 ps.[17] The reason for this spread of experimentally determined LO-phonon lifetimes seems to have two sources. Firstly, the quality of the sample surface can strongly influence the decay dynamics within the thin light-absorption layer.[18] Secondly, the decay rate of a nonthermal phonon population might contain strong contributions from the reabsorption by the photogenerated carriers of the initially excited phonons. This point will be discussed in detail later. Our choice of τ_{op} equal to 7 ps at 77 K and 3.5 ps at 300 K is in agreement with the most recent experimental results.[19,20]

Several theoretical approaches for the solution of Eqs. (1) and (2) have been presented in the literature. Details about the various methods can be found in Refs. 5–8 and 10–13. Certainly one of the most interesting methods is that of Collet and co-workers,[21] who directly solved the coupled transport equations through a discretization in **q** space and in time to obtain the evolution of the carrier and phonon distributions and of the mean electron-hole plasma energy during and after 80-fs laser excitation pulses of varying intensity. Another method, based on the carrier-temperature concept, is of particular interest here since it originated the Monte Carlo (MC) investigation of phonon perturbations. In this approach to dc field transport, the carriers are assumed to be characterized by a heated and drifted Maxwellian (HDM) distribution.[11] In the first attempt to use a MC technique in the

study of phonon perturbations, an iterative hybrid procedure was developed that coupled the HDM scheme to a one-particle MC simulation of non-Ohmic transport.[22,23] The full consistent Monte Carlo simulation, developed for the case of photoexcitation in GaAs,[24,25] will be presented in the next section.

A two-valley (at points Γ and L) model is used for GaAs (under the conditions considered here, X valleys do not contribute significantly). The following scattering mechanisms are considered: (1) deformation potential coupling to acoustic phonons ($D_{ac}=7$ eV), treated exactly according to the procedure given in Ref. 26; (2) unscreened polar-optical coupling to LO phonons; (3) unscreened scattering from ionized impurities, treated in the Conwell-Weisskopf formalism as given in Ref. 26. Throughout the paper, nominally undoped materials (with a residual impurity concentration of 10^{14} cm^{-3}) will be considered; (4) deformation potential coupling to intervalley $\Gamma \rightarrow L$ phonons ($D_{iv}=8\times10^{8}$ eV/cm); and (5) electron-electron scattering between Γ-valley electrons, which has been included using the algorithm presented in Ref. 27.

III. THE MONTE CARLO ALGORITHM

We present here an ensemble MC algorithm for the study of nonequilibrium phonon effects on the relaxation rate of photoexcited electrons. This procedure allows us to follow the time evolution of the phonon distribution. A collection of results has already been presented in Refs. 24, 25, 28, and 29.

The laser excitation is reproduced by adding particles to the simulation, distributed in time according to the line shape of the laser pulse, as shown in the inset of Fig. 3. The simulation is subdivided in time intervals Δt (with Δt typically much shorter than the average scattering time for the LO-phonon scattering). At time $T=j\,\Delta t$, the number of Monte Carlo electrons is updated from the previous step according to the expression

$$N_{\mathbf{q}}(T)=N_{\mathbf{q}}(T-\Delta t)+C\,\Delta t\cosh^{-1}(\omega_0 T)\ , \tag{5}$$

where ω_0 and C are the parameters which model the width and power of the laser pulse.

Electrons are excited in the conduction band centered around a given energy E_{inj}, with a small broadening depending on the width of the laser pulse (typically around 20 meV). Since the excitation energies considered here are below the threshold for intervalley scattering (0.3 eV for Γ to L transitions), there is no significant transfer to the satellite valleys.

The disturbances of other types of phonons are negligible in the situation examined here. The LO-phonon distribution function is followed in its time evolution, and phonon-induced modifications to the relaxation rates of the electrons are considered. In a finite-difference scheme, Eq. (2) for the phonon evolution can be written in the form

$$N_{\mathbf{q}}(n\,\Delta t)=N_{\mathbf{q}}((n-1)\Delta t)+\delta N_{\mathbf{q}}(n\,\Delta t)|_{\text{ph-}c}-[N_{\mathbf{q}}(n\,\Delta t)-N_L]\frac{\Delta t}{\tau_{op}},\quad n=1,2,3,\ldots\ . \tag{6}$$

The procedure set up to account for the LO-phonon disturbances has the following features.

(i) The time evolution of the LO-phonon distribution $N_{\mathbf{q}}$ is calculated as a function of wave vector $\mathbf{q}$ from the MC simulation, by setting up a histogram $h_{\mathbf{q}}$ defined over a grid in $\mathbf{q}$ space of mesh size Δq. After each scattering event involving a LO phonon, the histogram is updated. In the absence of external dc fields, because of the full spherical symmetry only the amplitude of $\mathbf{q}$ is relevant, thus reducing the complexity and the storage requirements of the simulation. Preliminary results for the field-dependent case have been presented recently.[30] A detailed analysis of such a situation will be given in paper II.[15]

(ii) At fixed times $T=j\,\Delta t$ during the simulation, N_q is calculated as

$$N_q(j\,\Delta t)=\bar{N}_q(j\,\Delta t)+[\bar{N}_q(j\,\Delta t)-N_L]\frac{\Delta t}{\tau_{op}}\ , \tag{7}$$

where

$$\bar{N}_q(j\,\Delta t)=N_q((j-1)\Delta t)+A\,\Delta h_q\ . \tag{8}$$

The term $A\,\Delta h_q$ gives the dynamical contribution of the electronic processes to the phonon distribution during the time step Δt. Here, Δh_q is the contribution of the c-ph processes to the histogram, and A is a normalization factor accounting for the density of states in $\mathbf{q}$ space and for the concentration of excited electrons, given by

$$A=\frac{2\pi^2 n_0}{q^2\,\Delta q\,N}\ , \tag{9}$$

where n_0 is the electron concentration and N the number of simulated particles.

The second term on the right-hand side of Eq. (7) accounts for phonon decays during Δt due to phonon-phonon processes. The algorithm for the phonon counting can be viewed as a hybrid MC solution of the phonon Boltzmann equation within a finite-difference scheme.

(iii) To account for the modifications induced by the phonon disturbance on the rate of electron-phonon scatterings, the integrated scattering probabilities for LO phonons are calculated and tabulated at the beginning of the simulation using an artificially high value N_{max} for the phonon distribution. The choice of the final state of each scattering process involving a LO phonon is made using a rejection technique which compares the actual value of the differential scattering rate with the maximized one. In this way, we are able to discriminate between the scatterings that can be attributed to the enhanced phonon distribution versus those induced by the initial maximization (which are treated as self-scatterings in the simulation). A schematic plot of the rejection technique is presented in Fig. 2. In order to reduce the number of self-scattering events, it is possible to recalculate the scattering rates at fixed times during the simulation. A numerical integration over the perturbed phonon distribution function gives the exact scattering rates at a given time, which can be used directly on the simulation.

The suggested procedure is a full MC simulation of the

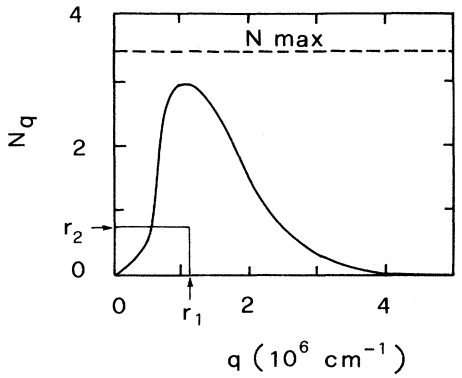

FIG. 2. Schematic of the rejection technique used for the selection of the final state in the Monte Carlo algorithm for hot-phonon effects. The two random numbers r_1 and r_2 are uniformly distributed in the range $(0,q_{max})$ and $(0,N_{max})$, respectively. The case illustrated in the figure represents an accepted scattering event.

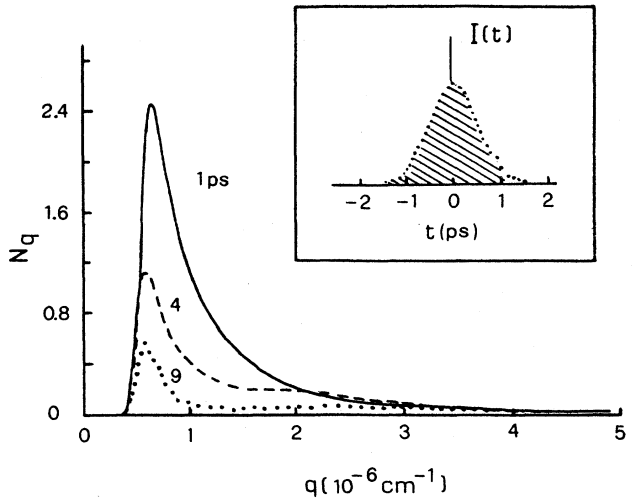

FIG. 3. Nonequilibrium LO-phonon distribution functions at three different delay times as a function of the phonon wave vector. The inset shows the shape of the laser pulse.

dynamics of an interacting electron-phonon gas within the finite-difference scheme indicated above, free of adjustable parameters. In the next section, the results of the MC simulation in the presence of laser excitation will be presented. The application of the algorithm in the presence of an applied electric field will be presented in a separate contribution. In that case, a two-dimensional grid, which stores the amplitude of **q** as well as the angle between **q** and the electric field, is used to describe the perturbed distribution.[15]

IV. SIMPLE CASE: EXCITATION FROM A SINGLE VALENCE-BAND LEVEL

A. Bulk GaAs

The algorithm described in the previous section has been applied to various situations to study the dynamics of the LO phonon, of the electron distributions, and their mutual effects. The time evolution of the perturbed phonon distribution is shown in Fig. 3 for an excited carrier density of 5×10^{16} cm^{-3}. Electrons are excited at an energy of 0.25 eV above the bottom of the conduction band, corresponding to a photon energy of 1.8 eV. The lattice temperature is 77 K. The line shape of the laser pulse is shown in the inset (half-width 0.8 ps). The LO distribution is driven out of equilibrium even during the excitation, due to the fast power dissipation of the high-energy photoexcited electrons. The maximum is reached at a delay time of 1 ps for wave vectors of about 6×10^5 cm^{-1}. The small q values that are amplified during and immediately after the excitation are due to the polar nature of the electron-phonon coupling. At longer times, the phonon distribution relaxes towards its equilibrium value as a result of two distinct processes, phonon reabsorption and phonon-phonon interaction. The first one is due to the fact that the group velocity of optical phonons is very small (less than 10^3 cm/s), implying that the phonons cannot drift away from the excitation volume during their lifetime. Therefore, if the phonon lifetime is long enough and the coupling with the carriers sufficiently strong, emitted phonons can be reabsorbed.

It is important to notice that modes of different wave vector evolve in time in different ways, as indicated in Fig. 4. Those with the smaller q (6×10^5 cm^{-1}) exhibit an exponential decay, immediately after the end of the excitation, with a characteristic decay time of 7 ps. At intermediate q's (8×10^5 and 10×10^5 cm^{-1}) the phonon distribution decays much faster at short times (up to 5- and 8-ps delay), approaching then the exponential behavior. The amplification of these large-q phonons is not as pronounced as that of the small-q ones.

The time evolution of the phonon distribution reflects

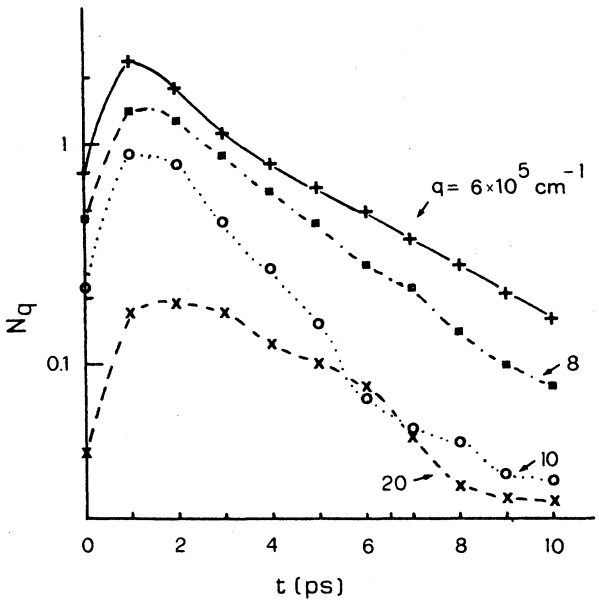

FIG. 4. Time evolution of four different modes as a function of delay time.

the microscopic details of the cooling processes in the coupled electron-phonon system. While phonon-phonon processes are always active, and their effect is independent of wave vector, phonon reabsorption varies drastically as a function of time and wave vector. In fact, the very rapid changes in the electron distribution function (which will be examined later) modify the range of phonon transitions that are allowed by energy and momentum conservation. Figure 5 shows the minimum q for LO-phonon absorption and emission as a function of electron energy in a parabolic band. At high energy, electrons can emit phonons with very small q, but as they cool the minimum allowed q shifts to higher values. Such a shift appears in Fig. 3, although it is hidden by the strong initial amplification. Furthermore, an electron will not be able to reabsorb the earlier emitted phonons once it goes below a certain energy.

This simple analysis explains why the phonons with small q vector excited during the first stages of the electron relaxation (up to 2-ps delay time) cannot be reabsorbed, and decay exponentially via nonelectronic phonon-phonon processes. On the other side, both the reabsorption and the phonon-phonon terms will contribute to the damping of phonons of larger wave vector in the first few picoseconds, leading to their faster decay over this time interval.

The modification of the scattering rates for the electron–LO-phonon interaction due to the phonon perturbation is presented in Fig. 6. There the total scattering rates for absorption and emission, obtained from a numerical integration over the perturbed distribution function N_q, are plotted at different time delays after the end of the laser pulse. Since at low temperature the value of the equilibrium phonon distribution is much smaller than unity, the emission probability is a few orders of magnitude higher than the absorption one. As the phonon population grows out of equilibrium, the absorption rate increases dramatically, relatively much faster than the emission one. The changes of the scattering rate with time reflect the temporal evolution of the phonon population. It is important to notice that even a few picoseconds after the pulse, a significant amount of phonons are still present and a considerable number of phonon reabsorptions is detected.

The time evolution of the electron distribution function, shown in Fig. 7, completes the previous analysis of

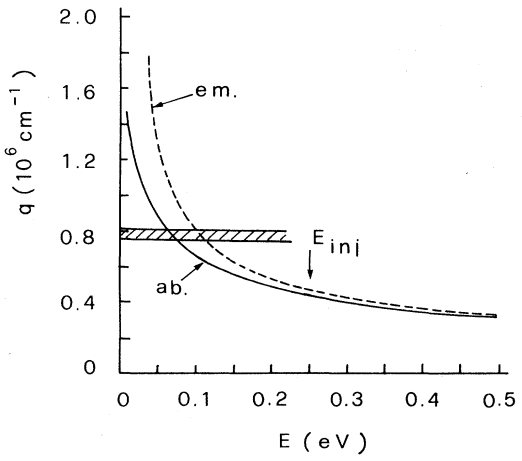

FIG. 5. Energy dependence of the minimum wave vector for absorption and emission of LO phonons as a function of energy in a parabolic band. The shaded area indicates typical Raman-active phonon wave vectors and E_{inj} is the energy value at which carriers are initially injected measured from the bottom of the conduction band.

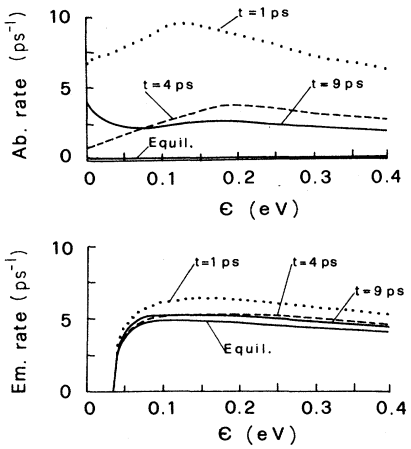

FIG. 6. Total scattering rates for polar-optical interaction at different times after the excitation as compared with their equilibrium value.

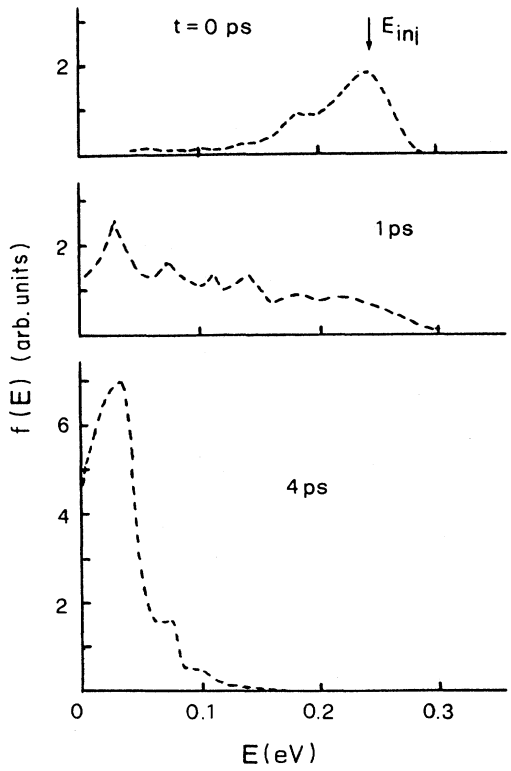

FIG. 7. Electron distribution function of carrier energy at different delay times.

the phonon amplification. The distinct peaks in the distributions at short time delays (0 and 1 ps) are due mainly to LO-phonon emission which sets in already during the laser pulse (an average time of 160 fs for the emission of a LO phonon by electrons at the excitation energy is calculated from the simulation). At a time delay of 4 ps, the electrons mainly populate the low-energy region below 100 meV. Many of them have an energy below the threshold for LO-phonon emission. It will be seen later that in this case reabsorption can become very important.

As a last remark on the phonon dynamics, it is important to compare the previous considerations with the experimental results of Raman spectroscopy. The shaded area in Fig. 5 indicates the range of Raman-active wave vectors for the data given in Refs. 19 and 31. The MC result for those modes (curve ■ in Fig. 4) is in good qualitative agreement with the findings of Kash *et al.*,[19] obtained for the same electron concentration but a higher excitation energy.

The effect of the phonon perturbation on the cooling of the photoexcited electrons is shown in Fig. 8. The electron relaxation rate is drastically reduced because of the presence of nonequilibrium phonons. The phenomenon is mainly due to the reabsorption of the LO phonons that have been emitted in the first stage of the relaxation without having had enough time to decay. The effect of phonon reabsorption grows with time as the electrons populate the low-energy regions below the threshold for optical emission. Furthermore, the reduction in the cooling rate of the electrons is even larger at higher electron densities or higher injection levels, as found both experimentally[2,4] as well as in our simulation.

The MC algorithm presented here has been compared with the models of Refs. 5 and 21. At the low excitation energies used in Ref. 21, the phonon disturbance is reduced with respect to the case shown in Fig. 3, and reaches its maximum at higher q's. The result of the simulation obtained with an electron density of 10^{16} cm^{-3} and an 80-fs laser pulse with an initial electron energy of 80 meV is shown in Fig. 9. The MC result agrees quite well with that of the more sophisticated model of Ref. 21.

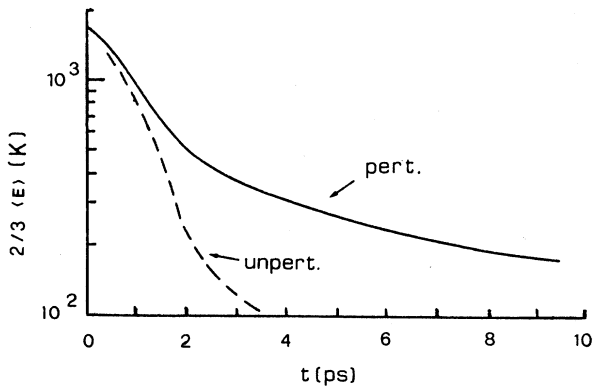

FIG. 8. Average electron energy, measured in equivalent temperature, as a function of time with (solid curve) and without (dashed curve) hot phonons.

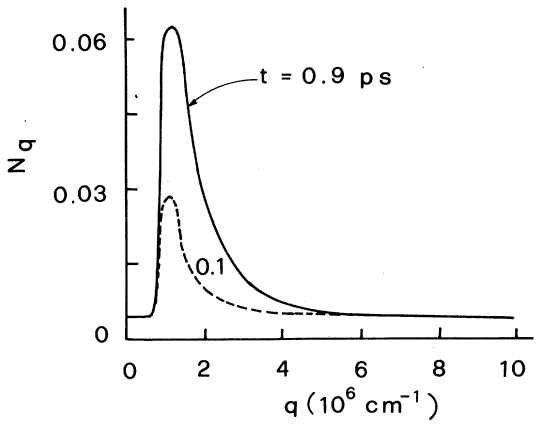

FIG. 9. Nonequilibrium phonon distribution for an excitation energy of 80 meV and an electron concentration of 10^{16} cm^{-3} for an 80-fs laser pulse at two different delay times.

The temperature model of Ref. 5 assumes that the carriers (electrons and holes) are characterized by a Fermi-Dirac distribution at any time during and after the laser pulse, corresponding to a very fast thermalization with the photogenerated plasma. In order to verify the consistency of our results, we have performed a simulation by assuming that the carriers are initially distributed according to a heated Maxwellian distribution. The MC results, obtained using the same parameters as in the calculation of Fig. 3, indicate in this case a much smaller phonon perturbation, with the maximum of the phonon distribution still reached at 1-ps delay time as in Fig. 3, but its value being reduced by a factor 2. The reduction of phonon heating is related to the population of the low-energy region of the Maxwellian distribution as compared to the sharp distribution at the excitation energy. The MC results agree very well with those we obtained from a temperature model for a one-component plasma. When both electrons and holes are considered, the temperature model, assuming the same temperature for both carriers, implies an inherent instantaneous energy transfer from the electrons to the holes, and thereby a further reduction of the phonon heating by electrons. Although the latter result depends heavily on the assumptions of the single-temperature model, it nevertheless shows that the electron-hole interaction can be very important. A preliminary step to combine the effect of electron-hole scattering and nonequilibrium phonons has recently been presented both for a two-temperature model[13] and a MC analysis.[32]

Up to now we restricted our discussion to cases where only the central valley is important. In general, especially if the excitation energy is sufficiently high, the population of the higher valleys (L and X) is not negligible. For such cases the influence of the satellite valleys on the phonon disturbances can be very strong. Figure 10 shows the minimum q for LO-phonon absorption and emission as a function of electron energy for the Γ (same curve as Fig. 5) and L valleys. Due to the higher effective mass of the latter valleys, the emitted LO phonons have a large wave vector. Because of the increased area of phase

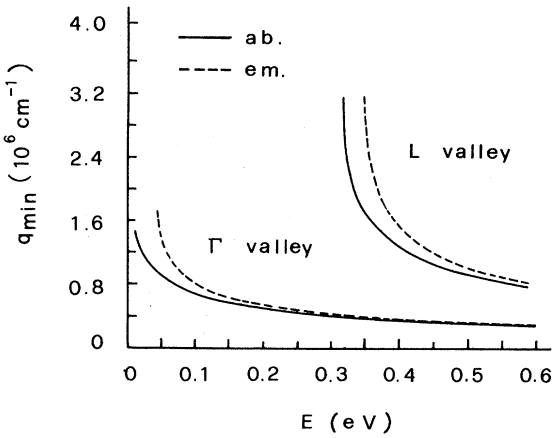

FIG. 10. Minimum wave vector for absorption and emission of LO phonons as a function of energy in a parabolic band for the Γ and L valleys of GaAs.

space, the contribution of the L electrons to the phonon distribution function will be reduced. This is illustrated in Fig. 11, where an initial electron energy of 0.5 eV has been used (with a Γ-L separation of 0.3 eV). The parameters of the simulation are the same as before. One picosecond after the excitation, about 60% of the electrons are found in the L valley. The MC histogram [Fig. 11(a)] confirms that the emission of LO phonons by L-valley electrons is concentrated in the large-q region. The actual number of phonons reflects indeed the relative population of the two valleys. Nevertheless, the effect of those phonons on the perturbed distribution [Fig. 11(b)] is negligible. Furthermore, all of the L-valley phonons have q values too large to be detected spectroscopically. We can therefore expect that phonon amplifications experimentally detected would decrease in the presence of substantial intervalley transfer. We are assuming here that the four ellipsoidal valleys can be represented by an equivalent spherical valley with an average effective mass, although a study of the effect of the valley anisotropy is needed.

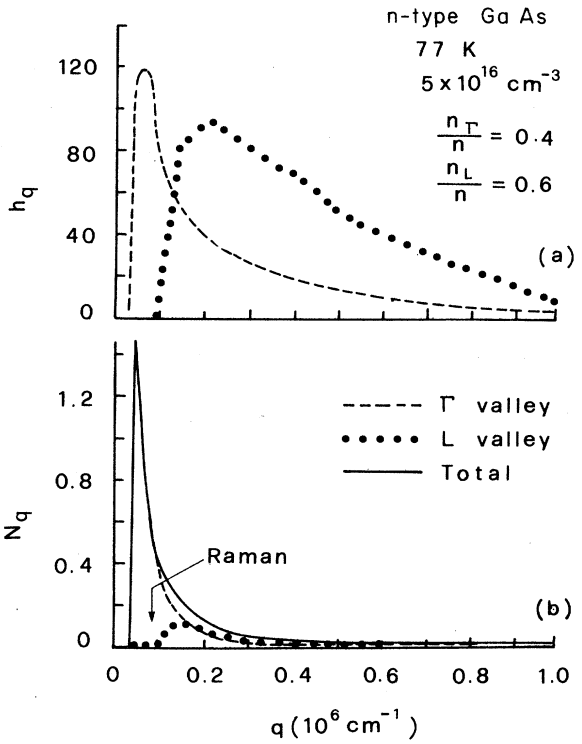

FIG. 11. (a) Phonon histogram and (b) distribution function at 1 ps after the excitation, for an initial electron energy of 0.5 eV.

B. GaAs-$Al_xGa_{1-x}As$ quantum wells

Recent results obtained with time-resolved photoluminescence have shown dramatically reduced energy relaxation rates for photoexcited electrons in GaAs-$Al_xGa_{1-x}As$ quantum wells.[3,33] It is still a debated question whether the slow cooling rates are due to the effect of nonequilibrium phonons,[4,29,34,35] of screening,[36,37] or of some combined action of these mechanisms. The algorithm just presented has been applied to a single quantum well of GaAs-$Al_xGa_{1-x}As$ (150 Å wide and 0.28 eV deep), with subband energies given by the solution of the one-dimensional wave equation for a square-well potential. The bands are assumed to be parabolic. The scattering rates (both intrasubband and intersubband) of the quantized 2D electrons with bulk unscreened LO phonons are calculated numerically without the use of momentum-conserving approximations.[38] It has been shown[38] that, for wells larger than 100 Å, there is little difference between the scattering rates calculated accounting for phonon confinement (slab modes) and the one obtained using bulk modes. Intervalley transfer to the L valleys (also quantized) is included as well. The mechanism of 2D electron-electron scattering is introduced in the MC simulation through a generalization of the self-scattering technique given in Ref. 39 to the multisubband quantized system.[40] The various electrons are allowed to interact via a statically screened Coulomb interaction determined by the long-wavelength limit of the two-dimensional Lindhard dielectric function. Degeneracy effects due to the Pauli exclusion principle are also considered.[40–42] In the present simulation we have neglected electron-hole scattering and recombination, which might be of importance in some of the reported experiments.

In two dimensions, the component of the phonon wave vector in the direction of the well, q_z, is not conserved due to the spatial localization of the electrons there. In fact, the emitted phonons are spatially localized, which causes problems as to their representation in terms of plane waves, as was noted by Price.[43] This problem has been more recently addressed by Cai *et al.*,[12] who solve the coupled 2D electron-phonon kinetic equations considering off-diagonal contributions of the phonon density matrix. In our model we considered a simpler approach, that is, that the q_z components of the phonon distribution are localized in a region of wave-vector space of extent $1/L$, L being the width of the well. This choice is indi-

cated by the probability amplitude for emission and absorption obtained from the 2D electron-phonon scattering matrix element which has been shown to be a zeroth-order spherical Bessel function of width $1/L$.[38,43] We approximate this function by a flat distribution over the range $1/L$. For intrasubband transitions, this function is centered around $q_z=0$, whereas for intersubband transitions, it is centered around a nonzero momentum related to the change in subband energy.[29] Therefore, the phonon distribution is tabulated for discrete q_z corresponding to the various intersubband and intrasubband events, with the phonon wave vectors otherwise treated as two dimensional.

The cooling of photoexcited electrons in an n-type GaAs-$Al_xGa_{1-x}As$ quantum well at low temperature (5 K) has been considered.[29,40,44] A background sheet density of 2.5×10^{11} cm^{-2} is used. The injected sheet density is 5×10^{11} cm^{-2}. The GaAs parameters are the same as for the bulk case. The width of the simulated laser pulse is about 1 ps, during which time carriers are added to the simulation with an initial energy of 0.25 eV above the bottom of the lowest subband. The inset in Fig. 12 shows the position of the energy levels in the well. Figure 12 shows the evolution of the electron total energy (kinetic plus potential) as a function of time during and after the pulse. The excited electrons lose energy mainly through the interaction with the background electrons and through the emission of LO phonons. For equilibrium phonons (□), the hot electrons are found to reach equilibrium in about 3 ps. In contrast with the case of an unperturbed phonon distribution, a much slower relaxation is found when nonequilibrium phonons are accounted for (○,△). The two cases in Fig. 12 correspond to different

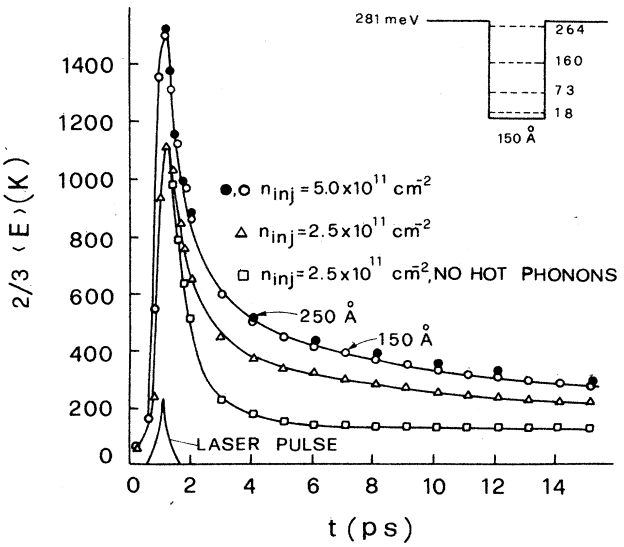

FIG. 12. Average electron energy, measured in equivalent temperature, as a function of time during and after the laser excitation for two different excitation sheet densities. The position of the energy levels in the well is shown in the inset.

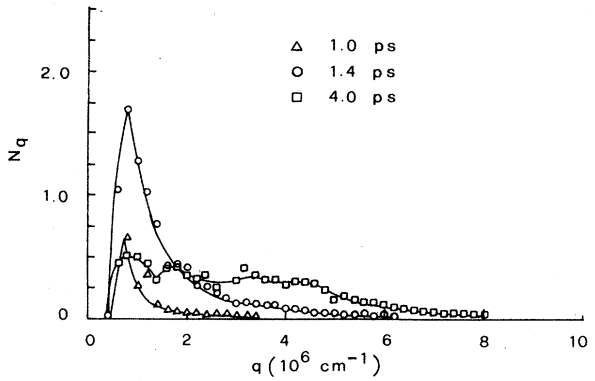

FIG. 13. LO-phonon distribution as a function of total parallel momentum (for $q_z=0$) for times during and after the laser excitation.

injection densities. At the excitation energy considered here, virtually no intervalley transfer occurs. It is worth noticing that no real dependence on well width has been found in the MC results.[29] The reduction of the electron cooling rate is due to the reabsorption of nonequilibrium phonons which build up during the initial pumping and the first stage of the electron relaxation. This is evidenced by the time evolution of the phonon distribution at $q_z=0$ (intrasubband scattering) shown in Fig. 13. The same, although reduced, features are found also at $q_z\neq0$. LO-phonon emission during the pulse and immediately after creates a large population of phonons at small q's. At longer times, phonon reabsorptions and phonon-phonon losses drive the distribution back to equilibrium. The secondary peak that develops at later times in the phonon distribution is due to phonon emission by electrons that have already relaxed to lower energy. As pointed out before, the reduction in the electron relaxation rate is mainly due to reabsorption of the emitted LO phonons. The effect is stronger when a considerable number of electrons have relaxed to the low-energy region below the emission threshold.

Recently, a time-resolved Raman analysis of the development of nonequilibrium LO phonons in narrow $Al_xGa_{1-x}As$-GaAs quantum wells was presented.[45] There, electrons were excited in the first subband with an excess energy of about 160 meV. From the anti-Stokes peak of the Raman signal it was possible to monitor the buildup of the nonequilibrium LO-phonon population. For an experiment performed in backscattering geometry in a two-dimensional system, the output (that is, the LO-phonon population) constitutes an average over all LO modes, contrary to the bulk case where a well-defined region of q space is analyzed.[45] The experimental results (extracted from the time-resolved average of the anti-Stokes peak) indicate an "average" phonon lifetime of 8 ps at 10 K. The MC results for the same situation are shown in Fig. 14 for three different values of τ_{op}.

It is clear that reabsorption plays a very important role in the experiment. The more strongly amplified phonons (around $q\simeq8\times10^6$ cm^{-1}) decay with a time constant which is much shorter than the ph-ph value introduced

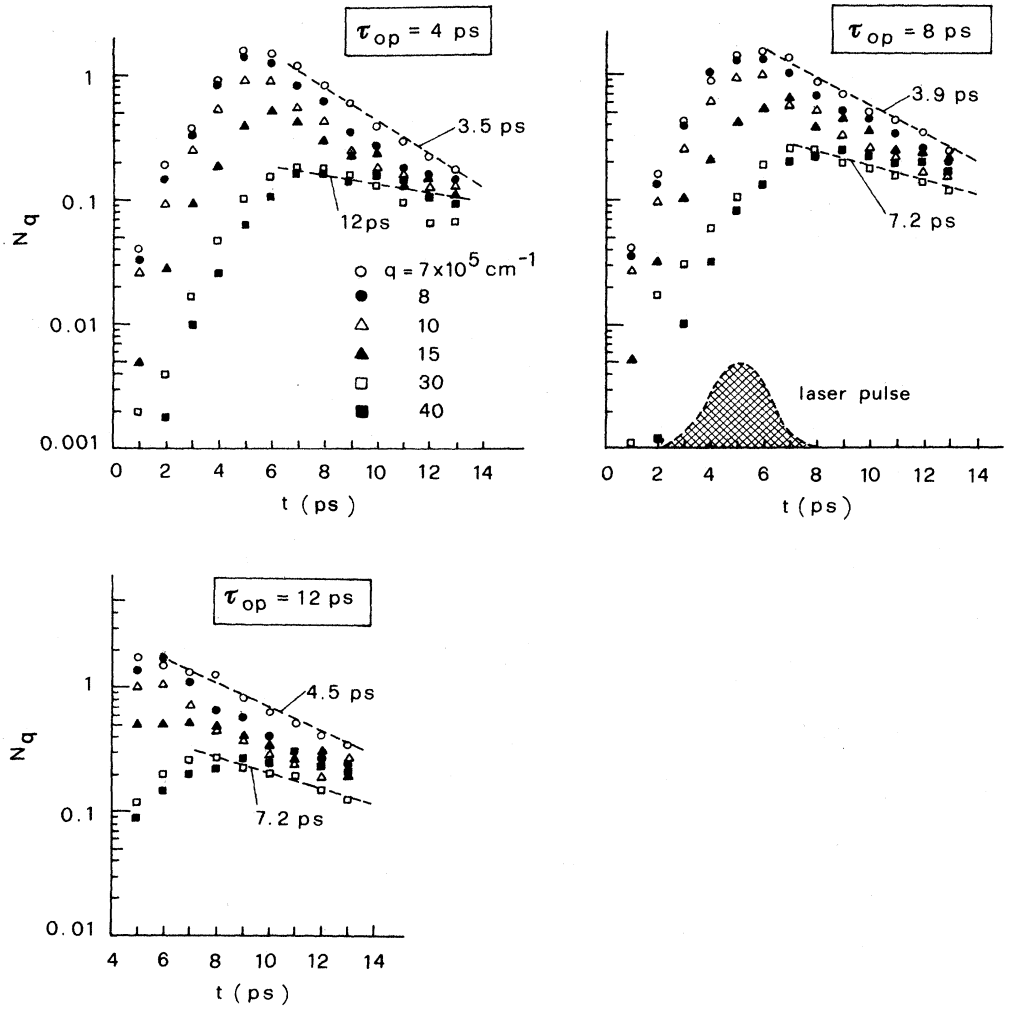

FIG. 14. Time evolution of various phonon modes obtained by using three different values for τ_{op}.

in the simulation. As pointed out in the discussion for the bulk case, this indicates a strong contribution of the electronic processes to the phonon lifetime. Therefore, even if it is hard to extract an average phonon lifetime from the results of Fig. 14, this seems to indicate that the measured phonon lifetime is not directly the nonelectronic ph-ph lifetime, but sets a lower limit for it.

V. REALISTIC MODEL: EXCITATION FROM A THREE-VALENCE-BAND MODEL

When the details of the band structure are taken into account for the photoexcitation process, a more elaborate description of the initial carrier distribution is necessary. As illustrated in Fig. 15 for bulk GaAs, the absorption of photons with considerable energy (typically around 2 eV)

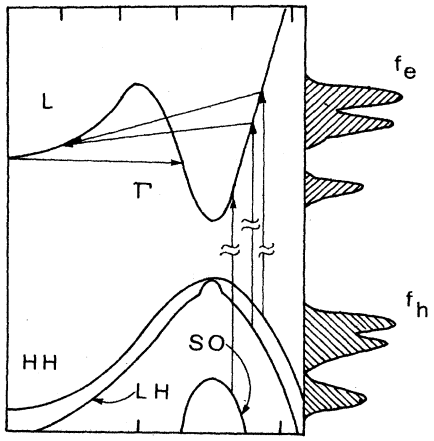

FIG. 15. Schematic representation of the excitation process in polar semiconductors.

induces transitions from the three hole bands. Therefore, the energy distribution of the photoexcited electrons is characterized by three distinct peaks, slightly broadened because of the warping of the valence band and of the natural absorption linewidth. This condition enters as the initial condition (for the electron energy distribution function) is the MC program described earlier. The present MC algorithm has been used to analyze the luminescence spectra after photoexcitation with a 400-fs-wide laser pulse at $T_L = 300$ K.[46,47] A very good agreement has been found with the experimental data for a Γ-L deformation potential $D_{\Gamma L}$ of $6.5 \pm 1.5 \times 10^5$ eV/cm. The physical parameters used in the simulation are shown in Table I. Figure 16 shows the MC electron distribution at three different time delays in bulk InP and GaAs. Some important differences are worth noticing. In GaAs, about 60% of the photoexcited carriers transfer to the satellite valleys during the laser pulse (the average time for $\Gamma \rightarrow L$ transition via phonon emission or absorption is about 80 fs). This creates the depletion in the high-energy region, above 0.3 eV, noticeable in Fig. 16. Carriers return slowly to the Γ valley, with a characteristic time of 2 or 3 ps. The net $\Gamma \rightarrow L$ transfer is actually a complicated series of processes where electrons can scatter in and out of the L valleys before leaving the actively coupled energy region (that is, the range of energy about 0.27 eV). The L valleys in InP are located at a much higher energy, and do not significantly contribute to the cooling process. The electron distribution is smoother than in GaAs, and the population of the low-energy region is higher at all times, since the cooling process is not slowed down by intervalley transfer. In both cases, electrons are characterized at the shortest time (1 ps) by an athermal distribution. Even if the intercarrier scattering is not sufficiently strong, at the low densities considered here (5×10^{16} cm^{-3}), to assure complete thermalization within the ensemble, it is nevertheless sufficient to smooth out the initially peaked distribution. This indicates the inadequacy even at the shortest times of the cascade model.[19]

TABLE I. Physical parameters used in the simulation.

	GaAs	InP
ε_g (eV)	1.42	1.34
m_e^Γ/m_0	0.063	0.078
m_e^L/m_0	0.22	0.4
m_e^X/m_0	0.58	
$\Delta_{\Gamma L}$ (eV)	0.3	0.61
$\Delta_{\Gamma X}$ (eV)	0.61	
ε_∞	10.92	9.52
ε_0	12.9	12.35
$D_{\Gamma L}$ (eV/cm)	7×10^8	2.5×10^8
$D_{\Gamma X}$ (eV/cm)	7×10^8	
D_{LX} (eV/cm)	5×10^8	
D_{ac} (eV/cm)	7×10^8	7×10^8
$T_{i\Gamma L}$ (K)	357	492
$T_{i\Gamma X}$ (K)	323	
T_{iLX} (K)	323	
T_{pop} (K)	410	498

The time behavior of the electron average energy for InP and GaAs is presented in Fig. 17 for three different carrier concentrations. The density dependence of the results is due to hot-phonon effects as described earlier. Clearly, other processes such as electron-hole scattering discussion in Sec. IV A or free-carrier screening of the

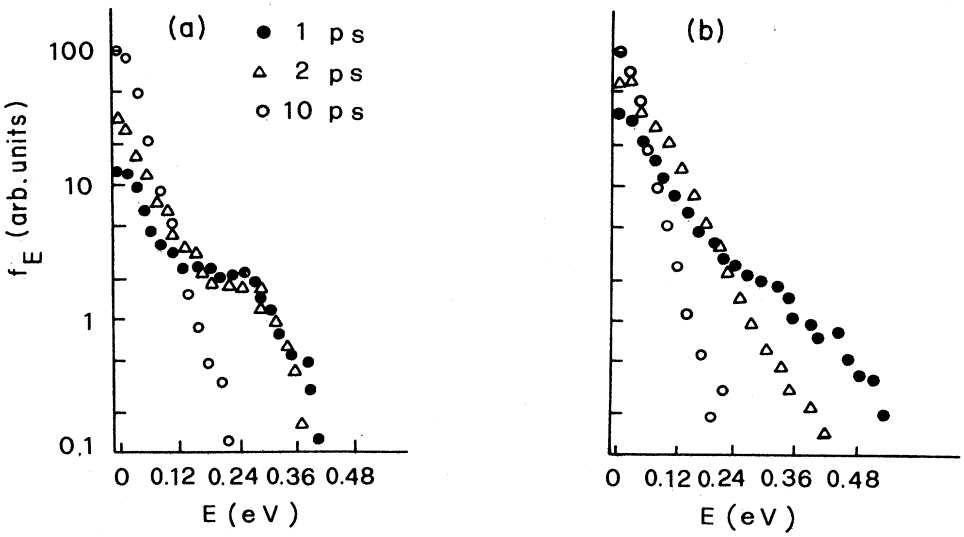

FIG. 16. Energy distribution function for Γ-valley electrons in (a) GaAs and (b) InP at three different time delays after the excitation. The excitation density is 5×10^{16} cm^{-3} and the lattice temperature is 300 K.

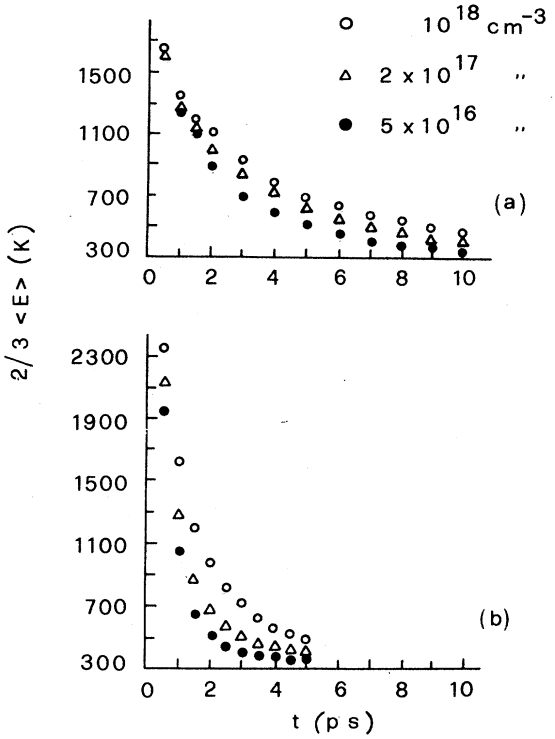

FIG. 17. Average energy, measured in equivalent temperature, of the Γ-valley electrons for different excitation densities in (a) GaAs and (b) InP at $T_L = 300$ K.

polar-optical-phonon coupling can have an influence on the carrier relaxation, especially at the highest carrier densities. However, screening has repeatedly been demonstrated to play a minor role in the presence of strong LO-phonon amplification.[5,11,15,48] At room temperature, the reduction of the cooling rate is not very pronounced, especially in GaAs, because of the large availability of LO phonons that limits the effectiveness of the reabsorption processes. The time behavior of the average energy indicates a very rapid cooling of the photoexcited electrons in InP, due to the confinement of electrons in the Γ valley and to the stronger polar coupling of this material. Because of the high density of Γ electrons, the hot-phonon effects noticeable in the first picoseconds after the excitation are stronger than in GaAs.

The characteristic behavior of the two materials also shows up in the nonequilibrium LO-phonon distributions shown in Fig. 18. A stronger and faster phonon buildup is found in InP, with the maximum amplification reached at a time delay of 1 ps. The time evolution of the Raman-active modes ($q_R \simeq 8\times10^5$ cm^{-1}) for GaAs is shown in Fig. 19. For the room-temperature case (open circles), a plateau is observed in the first picoseconds after excitation, which is direct evidence of the slow return of the electrons from the upper valleys. Such features are related to the fact that, within the spherical model for the upper valleys, phonons are emitted there with wave vectors outside the Raman-active area. Therefore, the contribution to the phonon amplification at q_R follows closely the loss of population of the upper valleys. The comparison of the time behavior of the phonon modes at two different temperatures is also presented in Fig. 19. After the initial delay, the populations decay with characteristic times of around 3.5 and 7 ps at 77 and 300 K, respectively, in agreement with the experimental results (see inset).

As a last point, we would like to comment on a previous determination of $D_{\Gamma L}$ for GaAs obtained from Raman data. In the experiment of Collins and Yu,[31] a value of $D_{\Gamma L}$ equal to 1.5×10^8 eV/cm was derived from the time evolution of the anti-Stokes peak for a much lower excitation density and a much longer laser pulse, compared to the situations examined above. The data were interpreted as indicating very little transfer of photoexcited carriers into the satellite valleys despite the very high excitation energy. Our MC simulation of that experiment shows that the nonequilibrium phonon population

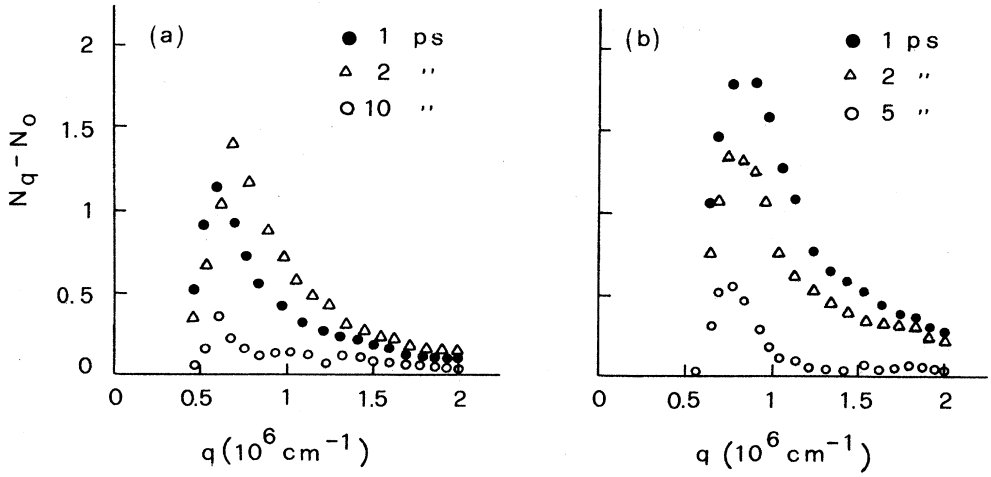

FIG. 18. LO-phonon distribution for Γ-valley electron in (a) GaAs and (b) InP for three different time delays after the excitation at $T_L = 300$ K.

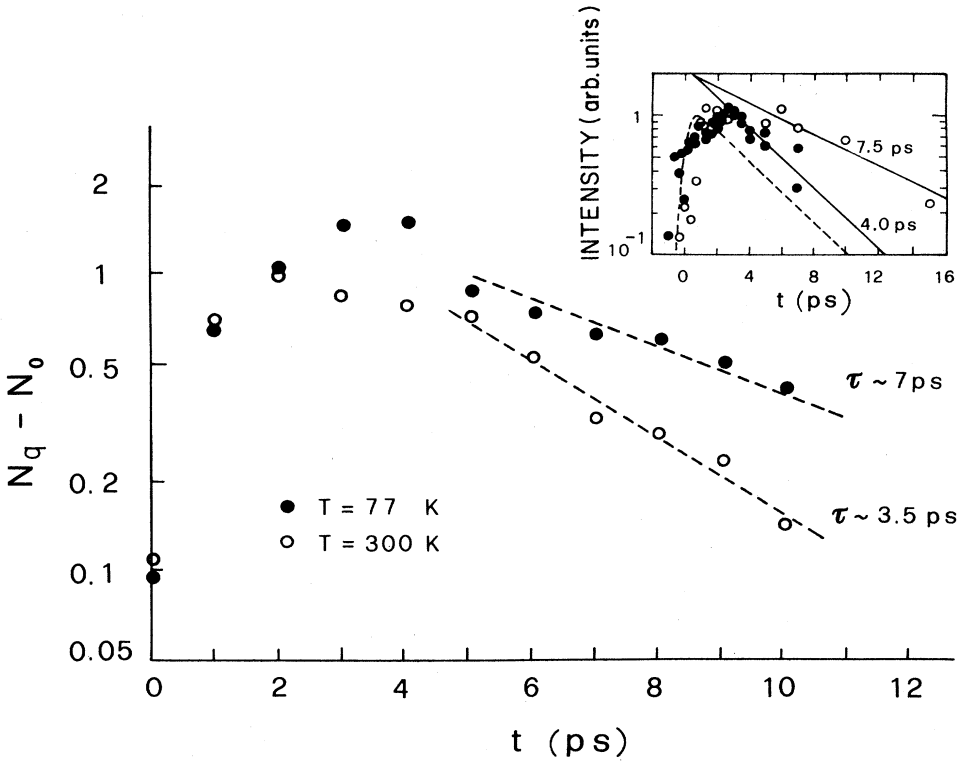

FIG. 19. Time evolution of the Raman-active modes for two different temperatures. The experimental results of Ref. 19 are shown in the inset.

is not very sensitive to the Γ-L coupling, as shown in Fig. 20, mainly because of the long times and small densities involved. Figure 21 illustrates this point, by comparing the time evolution of the phonon disturbance (at $q=8\times10^5$ cm^{-1}) obtained from the MC simulation with two values of $D_{\Gamma L}$ equal, respectively, to 1.5×10^8 and 7×10^8 eV/cm. When the Γ-L coupling is weak, the transfer of photoexcited electrons to the satellite valleys is drastically reduced. Therefore, a stronger phonon amplification is found at the shortest times, compared with the case ($D_{\Gamma L}=7\times10^8$ eV/cm) when the intervalley transfer is dominant.

As was shown in Ref. 46, the MC analysis of time-resolved photoluminescence data indicates that a value of $D_{\Gamma L}=1.5\times10^8$ eV/cm is far too low to interpret the experimental results, while an excellent agreement is found for $D_{\Gamma L}=6.5(\pm1.5)\times10^8$ eV/cm. If the experiment could be repeated under more favorable conditions (that

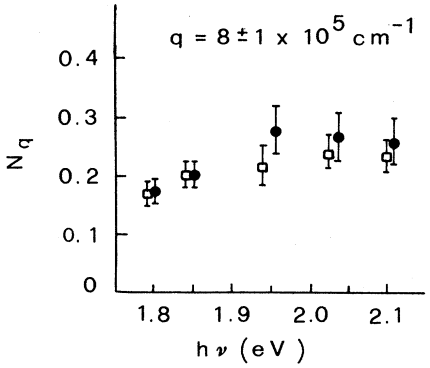

FIG. 20. Monte Carlo calculations of the Raman-active modes as a function of the laser-pulse energy under the condition of the experiment of Collins and Yu (Ref. 31) for two different values of the Γ-L coupling: □, $D_{\Gamma L}=7.0\times10^8$ eV/cm; ●, $D_{\Gamma L}=1.5\times10^8$ eV/cm.

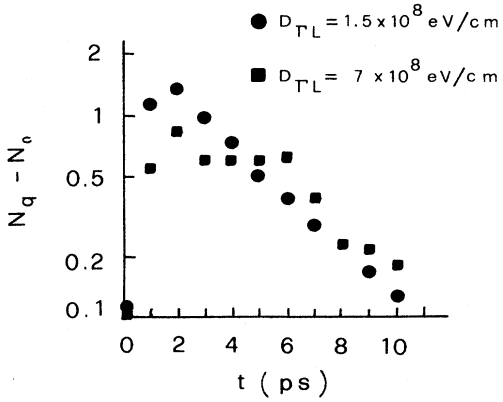

FIG. 21. Monte Carlo calculations of the Raman-active modes as a function of time under the condition of the experiment of Shah *et al.* (Ref. 46) for two different values of the Γ-L coupling: ■, $D_{\Gamma L}=7.0\times10^8$ eV/cm; ●, $D_{\Gamma L}=1.5\times10^8$ eV/cm.

is, with a much shorter laser pulse and a higher density), the phonon distribution could be used to discriminate between different values of $D_{\Gamma L}$.

VI. CONCLUSIONS

A full Monte Carlo technique for the study of electrons and phonon dynamics in bulk GaAs, InP, and in $Al_xGa_{1-x}As$-GaAs quantum wells has been presented. The method does not require any assumption on the form of the distribution function, and provides a detailed microscopic description of the transport phenomena. We have focused on the relaxation of electrons photoexcited by ultrafast laser pulses. During the initial stage of the relaxation, a strong emission of LO phonons occurs which drives the phonon distribution function out of equilibrium. The presence of a perturbed LO-phonon population causes a reduction of the cooling rate of the photoexcited electrons. Such a reduction, which is a function of the excitation conditions and of the lattice temperature, is caused by a sizable reabsorption of LO phonons by the cooling electrons. Peculiar differences in the time evolution of the electron and phonon distributions are found in GaAs versus InP, due to the contribution of the satellite valleys in the former material. The results of the Monte Carlo simulation compare favorably with available experimental results obtained with time-resolved photoluminescence and Raman measurements. A similar investigation for the case of bulk GaAs has recently been presented in Ref. 49. The slowing down of the photoexcited electrons due to the presence of hot phonons has also been found in GaAs-$Al_xGa_{1-x}As$ quantum wells.

ACKNOWLEDGMENTS

We would like to thank Dr. C. Jacoboni for helpful discussions. Partial support from the European Research Office and the Centro Interdipartimentale di Calcolo Automatico e Informatica Applicata (CICAIA) is gratefully acknowledged. This research is financed by Progetto Finalizzato Materiali e Dispositivi per l'Elettronica a Stato Solido (MADESS) del Consiglio Nazionale delle Ricerche (CNR).

[1] J. Shah, R. C. C. Leite, and J. F. Scott, Solid State Commun. **8**, 1089 (1970).
[2] K. Kash, J. Shah, D. Block, A. C. Gossard, and W. Wiegmann, Physica **134B**, 189 (1985).
[3] J. F. Ryan, R. A. Taylor, A. J. Turbefield, and J. M. Worlock, Surf. Sci. **170**, 511 (1986).
[4] K. Leo, W. W. Rühle, H. J. Queisser, and K. Ploog, Phys. Rev. B **37**, 7121 (1988).
[5] W. Pötz and P. Kocevar, Phys. Rev. B **28**, 7040 (1983).
[6] M. Pugnet, J. Collet, and A. Cornet, Solid State Commun. **38**, 531 (1981).
[7] P. J. Price, Physica **134B**, 165 (1985).
[8] P. Lugli, Solid State Electron. **31**, 667 (1988).
[9] E. Conwell, *High Field Transport in Semiconductors* (Academic, New York, 1967).
[10] R. Luzzi, J. Lumin. **30**, 318 (1985).
[11] P. Kocevar, J. Phys. C **5**, 3349 (1972); Physica B+C **134B**, 155 (1985).
[12] W. Cai, C. M. Marchetti, and M. Lax, Phys. Rev. B **35**, 1369 (1987).
[13] W. Pötz, Phys. Rev. B **36**, 5016 (1987).
[14] P. G. Klemens, Phys. Rev. **148**, 845 (1966).
[15] M. Rieger, P. Kocevar, P. Lugli, P. Bordone, L. Reggiani, and S. M. Goodnick, following paper, Phys. Rev. B **39**, 7866 (1989).
[16] D. von der Linde, J. Kuhl, and H. Klingenberg, Phys. Rev. Lett. **44**, 1505 (1980).
[17] Mooradian and G. B. Wright, Solid State Commun. **4**, 431 (1966).
[18] T. C. Damen, R. C. C. Leite, and J. Shah, in *Proceedings of the 10th International Conference on the Physics of Semiconductors,* edited by S. P. Keller, J. C. Hensel, and F. Stern (U.S. Atomic Energy Commission, Washington, D.C., 1970).
[19] J. A. Kash, J. C. Tsang, and J. M. Hvam, Phys. Rev. Lett. **54**, 2151 (1985).
[20] E. O. Gobel (private communication).
[21] J. Collet and T. Amand, J. Phys. Chem. Solids **47**, 153 (1986).
[22] P. Bordone, C. Jacoboni, P. Lugli, L. Reggiani, and P. Kocevar, Physica B+C **134B**, 169 (1985).
[23] P. Bordone, C. Jacoboni, P. Lugli, L. Reggiani, and P. Kocevar, J. Appl. Phys. **61**, 1460 (1987).
[24] P. Lugli, C. Jacoboni, L. Reggiani, and P. Kocevar, Appl. Phys. Lett. **50**, 1251 (1987).
[25] P. Lugli, C. Jacoboni, L. Reggiani, and P. Kocevar, Proc. SPIE **793**, 102 (1987).
[26] C. Jacoboni and L. Reggiani, Rev. Mod. Phys. **55**, 645 (1983); E. M. Conwell and V. F. Weisskopf, Phys. Rev. **77**, 388 (1950).
[27] P. Lugli and D. K. Ferry, Physica B+C **134B**, 364 (1985).
[28] P. Lugli, Phys. Scr. **T19**, 190 (1987).
[29] P. Lugli and S. Goodnick, Phys. Rev. Lett. **59**, 716 (1987).
[30] M. Rieger, P. Kocevar, P. Bordone, P. Lugli, and L. Reggiani, Solid State Electron. **31**, 687 (1988).
[31] C. L. Collins and P. Y. Yu, Phys. Rev. B **30**, 4501 (1984).
[32] M. A. Osman, M. J. Kann, D. K. Ferry, and P. Lugli, in *Picosecond Electronics and Optoelectronics II,* edited by F. Capasso, C. H. Lee, F. J. Leonberges, and H. Morkoç (Springer-Verlag, Berlin, 1987), p. 82.
[33] Z. Y. Xu and C. L. Tang, Appl. Phys. Lett. **44**, 692 (1984).
[34] S. Das Sarma, J. K. Jain, and R. Jakabert, Phys. Rev. B **37**, 4560 (1988).
[35] J. Shah, A. Pinczuk, A. C. Gossard, and W. Wiegmann, Phys. Rev. Lett. **54**, 2045 (1986).
[36] C. H. Yang, J. M. Carlson-Swindle, S. A. Lyon, and J. M. Worlock, Phys. Rev. Lett. **54**, 2045 (1986).
[37] S. Das Sarma, W. Y. Lai, and A. Kobayashi, in *Proceedings of the 19th International Conference on the Physics of Semiconductors,* edited by O. Engström (World Scientific, Singapore, 1987), p. 651.
[38] F. A. Riddoch and B. K. Ridley, J. Phys. C **16**, 6971 (1983).
[39] R. Brunetti, C. Jacoboni, A. Matulionis, and V. Dienys, Physica B+C **134B**, 369 (1985).
[40] S. M. Goodnick and P. Lugli, Phys. Rev. B **37**, 2578 (1988).
[41] S. Bosi and C. Jacoboni, J. Phys. C **9**, 315 (1976).

[42]S. M. Goodnick and P. Lugli, in *Proceedings of the 18th International Conference on the Physics of Semiconductors,* edited by O. Engström (World Scientific, Singapore, 1987), p. 1335.
[43]P. J. Price, Ann. Phys. (N.Y.) **133**, 217 (1981).
[44]S. M. Goodnick and P. Lugli, in *High Speed Electronics,* edited by B. Kallbak and H. Beneking (Springer-Verlag, Berlin, 1986), p. 116.
[45]J. Tsen (unpublished).
[46]J. Shah, B. Deveaud, J. C. Damen, W. T. Tsang, A. C. Gossard, and P. Lugli, Phys. Rev. Lett. **59**, 2222 (1987).
[47]P. Lugli (unpublished).
[48]P. Kocevar, in *Festkörperprobleme (Advances in Solid State Physics),* edited by P. Grosse (Pergamon, Braunschweig, 1987), Vol. 27, p. 197.
[49]R. Mickevicius and A. Reklaitis, Solid State Commun. **64**, 10 (1987); **64**, 1305 (1987).